CARBON letters

Original Articles
Carbon Letters Vol. 27, 50-63 (2018)

Potentiometric sensor of graphene oxide decorated with silver nanoparticles/molecularly imprinted polymer for determination of gabapentin

Nehad A. Abdallah[1,2,♠] and Heba F. Ibrahim[2]

[1]Pharmacognosy and Pharmaceutical Chemistry Department, Faculty of Pharmacy, Taibah University, Al-Madinah Al-Munawarah 41477, KSA
[2]Experiments and Advanced Pharmaceutical Research Unit, Faculty of Pharmacy, Ain Shams University, Cairo 1156, Egypt

Article Info

Received 15 November 2017
Accepted 27 December 2017

♠Corresponding Author
E-mail: nehad.amin@gmail.com
Tel: +966-560034928

Open Access

DOI: http://dx.doi.org/10.5714/CL.2018.27.050

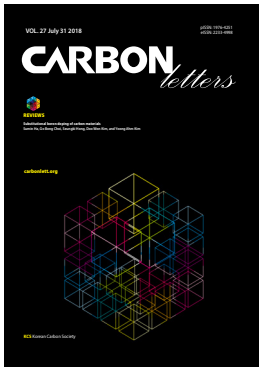

http://carbonlett.org

pISSN: 1976-4251
eISSN: 2233-4998

Abstract

An imprinted potentiometric sensor was developed for direct and selective determination of gabapentin. Sensor is based on carbon paste electrode adapted by graphene oxide that is decorated with silver nanoparticles and mixed with molecularly imprinted polymers nanoparticles using gabapentin as a template molecule. The synthesized nanoparticles were characterized by Fourier transmission infrared spectroscopy, transmission electron microscopy and X-ray diffraction. Under optimal experimental conditions, the studied sensor exhibited high selectivity and sensitivity with LOD of 4.8×10^{-11} mol L^{-1}. It provided a wide linearity range from 1×10^{-10} to 1×10^{-3} mol $L^{-1}$and high stability for more than 3 mo. The sensor was effectively used for the determination of gabapentin in pharmaceutical tablets and spiked plasma samples.

Key words: gabapentin, molecular imprinted nanoparticles, graphene oxide, sensor

1. Introduction

Gabapentin (GP; 1-(aminomethyl) cyclohexane acetic acid), shown in Fig. 1, is an anticonvulsant agent that is used in the treatment of epilepsy and management of neuropathic pain [1]. Gabapentin is structurally related to GABA and functions by interfering with calcium channels to alter transmitter release [2]. It is commonly used as an adjunctive therapy for partial seizures [3].

Different instrumental techniques have been reported for the quantitative determination of GP. As gabapentin has neither substantial ultraviolet (UV)-VIS absorption nor fluorescence emission, analysis of the drug has been attained through its derivatization to produce a chromophore, which can be measured by fluorescence or UV detectors. The most commonly used techniques are spectrophotometry [4-10], HPLC [11-18], LC-MS [19,20] and GC-MS [21]. Several electrochemical methods are applied for GP determination, including voltammetry [22-26] and potentiometry [27,28].

Potentiometric electrodes [27,28] are based on the formation of an ion pair complex between GP and either phosphomolybdic acid or phosphotungstic acid as the key element for GP recognition. These sensors provide limited sensitivity and selectivity with a long response time that reached 35 s. In addition, these sensors suffer from limited working pH range and short lifetime.

Molecularly imprinted polymer (MIP) is a synthesized polymer material, also called a man-made receptor for molecular recognition [29]. The cavities of MIP can memorize the structure and the positions of the functional groups complementary to the template molecule. This interaction is done via various non-covalent interactions, such as hydrogen bonds, ionic bonds and van der Waals interactions [30,31].

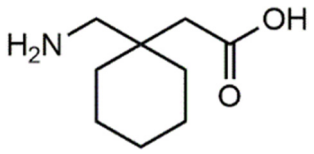

Fig. 1. Chemical Structure of gabapentin.

MIP sensors have the advantages of high selectivity, high sensitivity, low detection limit, ease of miniaturization and automation and low cost. These are due to the combination of the molecularly imprinted technique and electrochemical detection. Many molecularly-imprinted electrochemical sensors have been used for the determination of pharmaceutical drugs and insecticides [32-34]. An electrochemical response is obtained when the MIP membrane is recognized and united with the target molecules (i.e., template molecule or imprinted molecule); then, the electro-signal can be recorded and the concentration of the goal molecules can be determined. MIPs are functional sensing elements of MIP based sensors. These sensors can distinguish template molecules with high specificity based on the cavities in the spatial structure and binding sites in the MIP membrane, perfectly match to a specific target molecule. In the synthesis process, the template molecules interact with the monomer to form a multi-action spot, and the polymerization process is remembered. When the template molecules are detached, the cavities that match the spatial configuration of the template are obtained; they will then selectively identify the template molecules and their analog compounds [35].

Various substances can act as template molecules in the molecular imprinting technique. Typically, these molecules contain highly polar groups (such as carboxyls and aminos). It is easy to prepare high-performance MIPs because strong polar groups and functional monomers can form more stable molecular complexes. Due to the outstanding advantages of hydrogen bonds in terms of directionality, saturation and strength, MIPs with high selectivity and affinity can be produced from imprinted molecules that can form hydrogen bonds with functional monomers [36].

In this study, a carbon paste electrode (CPE) based on molecular imprinted polymer nanoparticles (MIP/NPs) was applied for the sensitive and selective determination of GP. MIP/NPs were synthesized by suspension polymerization to offer a highly active surface area. The studied electrode is based on the fabrication of a CPE modified with a graphene oxide and silver nanoparticle mixture (GO/Ag-NPs). The insulating effect of MIP-NPs can be minimized by the use of metal NPs in combination with graphene oxide. Graphene oxide is widely used in the electrochemical field owing to its easy synthesis and high dispersibility [37]. Silver is one of the best metal conductors. Silver ion is widely applied in the electrochemical field. It is characterized by good biocompatibility, and high electronic and catalytic properties. Ag-NPs improve the sensor stability and enhance the rate of the electron transfer in electrochemical reactions [38]. The combination of GO and Ag-NPs in electrochemical sensors offers great advantages including high surface area and the provision of fast mass transport to the binding sites, which lead to more rapid and sensitive response. GO is widely used in many chemical and biological sensors due to its high chemical stability, and its unique electronic and mechanical properties [39,40].

2. Experimental

2.1. Instrumentation

Potentiometric measurements were performed with CLEAN digital ion analyzer PH 600, model 007747 (China) and Heidolph MR Hei-Standard, magnetic stirrer model 100818877. The electrochemical cell was completed with the aid of an Ag/AgCl double junction reference electrode, model Z113107-1EA batch 310 (Sigma-Aldrich, USA).

2.2. Reagents

GP reference standard was kindly supplied by Delta Pharm for Pharmaceuticals, 10th of Ramadan, Egypt. Methacrylic acid (MAA), ethylene glycol dimethacrylate (EGDMA) and graphite powder were purchased from (Acros, Organics, USA). Azobisisobutyronitrile (AIBN) was purchased from (Merck, Germany), 3-mercaptopropyl trimethoxysilane (MPTS) was purchased from (Sigma Aldrich). $KMnO_4$, $NaNO_3$ and $AgNO_3$ were obtained from (Fluka, USA). All utilized solvents and reagents were of analytical grade.

2.3. Procedure

2.3.1. Preparation of standard GP solution

GP standard aqueous solution with a concentration of 1×10^{-2} mol L^{-1} was prepared in a 250 mL volumetric flask by weighing and dissolving 0.428 g of GP and completing the volume with deionized water. Working solutions of different concentrations from 1×10^{-3} to 1×10^{-11} mol L^{-1} were prepared by suitable dilution of the standard solution.

2.3.2. Preparation of MIP-NPs by suspension polymerization method

MIP-NPs were synthesized using silicon oil. In a screw-capped glass tube, 0.6 mmol GP and 6 mmol MAA were added and dissolved in 15 mL acetonitrile. The mixture was sonicated for 5 min to allow prearrangement. Thirty mmol EGDMA was added to the mixture with continuous stirring, followed by the addition of 0.1 mmol AIBN. The mixture was purged with N_2 gas and this was followed by the addition of 100 mL of silicon oil. The mixture was stirred at 600 rpm for 15 min to form small polymerizable droplets. The suspension was purged with N_2 gas for 15 min and heated at 70°C for 48 h to complete the polymerization process. The formed MIP-NPs were filtered and washed with petroleum ether. Leaching of the template molecules was done by washing with a mixture of methanol and acetic acid (9:1 v/v %) for 20 h until no template was detected using the reported HPLC method [18]. The leached MIP-NPs were dried under vacuum at 60°C for 24 h. The NIP-NPs were prepared using the same procedure without the addition of GP.

2.3.3. Synthesis of graphene oxide nanoparticles (GO-NPs)

GO-NPs were synthesized using the modified Hummers Jr. and Offemen method [41]. In a 250 mL beaker, 2 g of graphite powder was added to 1 g of $NaNO_3$; this was followed by subsequent addition of 50 mL of H_2SO_4 with continuous stirring in an ice-bath. Five grams of $KMnO_4$ was added slowly to the previous solution while the temperature was set at 25°C. The solution was heated at 35°C and 90 mL of water was added slowly. Reduction of the residual permanganate was performed by the addition of 5% H_2O_2 aqueous solution until bubbling disappeared. The formed GO was collected after centrifugation. The separated residue was washed with warm water several times until the pH of the suspension reached approximately seven. GO powder was obtained after freezing and drying the suspension. Fifty milligrams of the formed GO was added to 50 mL ethanol and ultrasonicated for 1 h. Two milliliters of MPTS was added slowly to the formed suspension to ease the surface assembly of Ag-NPs. The mixture was refluxed with continuous stirring at 65°C for 10 h. The produced particles were washed several times with ethanol and dried under vacuum.

2.3.4. Synthesis of Ag-NPs

The solid powder of 0.15 g $AgNO_3$ was dissolved in 120 mL of deionized water, stirred and boiled. Four milliliters of 1% sodium borohydride solution was added drop by drop while stirring. The finally-obtained solution was yellow green in color, indicating the formation of Ag-NPs. The heating was stopped and the solution was stirred until it had cooled and reached room temperature. The solution was filtered and the formed NPs were washed with deionized water and thereafter dried at 80°C for 4 h.

2.3.5. Synthesis of GO supported Ag nanoparticles

GO/Ag-NPs were prepared by adding 60 mg of the functionalized GO to 60 mL of deionized water and subjecting mixture to ultrasonication for 2 h. Fifteen millilters of the prepared colloidal Ag-NPs solution was added slowly and the mixture was again ultrasonicated for 15 min. The mixture was left at ambient temperature for 10 h and then centrifuged. The formed GO/Ag-NPs were collected, washed with deionized water and dried under vacuum.

2.3.6. Preparation of GP-CPE using mixture of GO/Ag-NPs and MIP-NPs

In order to prepare GO-modified CPE, 20 mg graphite powder was mixed with 35 mg GO/Ag-NPs and mixture was homogenized in a mortar; this was followed by the addition of 25 mg MIP-NPs and 0.02 g paraffin oil as a binder. The produced paste was used to fill the Teflon cavity of the electrode. By pushing the steel screw forward through the electrode body, a new surface was obtained, which was polished with clean filter paper to obtain a new, shiny surface. The electrode was kept in 1×10^{-5} mol L^{-1} of GP solution of pH 2 when not in use.

2.4. Binding study and entrapment efficiency of prepared MIP-NPs

Binding experiment was done by adding 20 mg samples of the produced MIP-NPs to 10 mL of GP solutions of varying concentrations. The mixtures were continuously stirred for 10 h at room temperature. The solid particles were separated by centrifugation at 3000 rpm for 15 min. The concentration of the free GP in the supernatant was determined by HPLC assay [18]. The bound GP was calculated by subtracting the free GP concentration from the initial concentration. The obtained results were used for Scatchard analysis. The entrapment efficiency and the drug loading capacity percentage were also calculated.

2.5. Sensor selectivity

The selectivity of the proposed sensor towards interfering ions was determined by calculating the potentiometric selectivity coefficient using the separate solution method [42] and applying the following equation;

$$log K_{A,B}^{pot} = \frac{(E_B - E_A)Z_A F}{(2.303RT)} + \left(1 - \frac{Z_A}{Z_B}\right) log[A] \quad (1)$$

, where $K^{pot}_{A,B}$ is the potentiometric selectivity coefficient. E_A is the potential measured for 1×10^{-4} mol L^{-1} of GP solution; E_B is the potential measured for 1×10^{-4} mol L^{-1} of the interfering solution. Z_A and Z_B are the charges of GP and the interfering substance, respectively. $2.303RT/Z_AF$ is the slope of the calibration plot (mV/ concentration decade). [A] is the activity of GP.

2.6. Determination of GP in bulk and pharmaceutical tablets

The electrochemical potential of GP was determined by the standard addition method [43]. Changes in potential readings were recorded after additions of small volumes of 1×10^{-3} mol L^{-1} standard GP solution to 50 mL samples of different concentrations.

Twenty tablets of Neurontin were weighed separately, ground and uniformly mixed. An amount of the powder equivalent to 0.428 g of GP was weighed and transferred to a 250 mL volumetric flask. About 100 mL of deionized water was added and the solution was sonicated for 10 min. The solution was filtered and completed to volume with deionized water. Several solutions of various concentrations ranging from 1×10^{-10} to 1×10^{-3} mol L^{-1} were prepared by suitable dilutions of the prepared solution. The solution potentials were measured using the proposed sensor and their concentrations were calculated from the corresponding regression equation.

2.7. Determination of GP in spiked human plasma samples

Using 5 mL stoppered volumetric flasks, 1.5 mL samples of plasma were added and spiked with different volumes of standard GP solution to provide different concentrations that ranged from 0.1 to 6 μg mL^{-1}, which are equivalent to 5.8×10^{-7} to 3.5×10^{-5} mol L^{-1}. The volumes were completed to the mark using citrate buffer pH 2. The solutions were mixed with continuous shaking for 5 min. After that, the solutions were transferred to 10 mL beakers for potentiometric measurements.

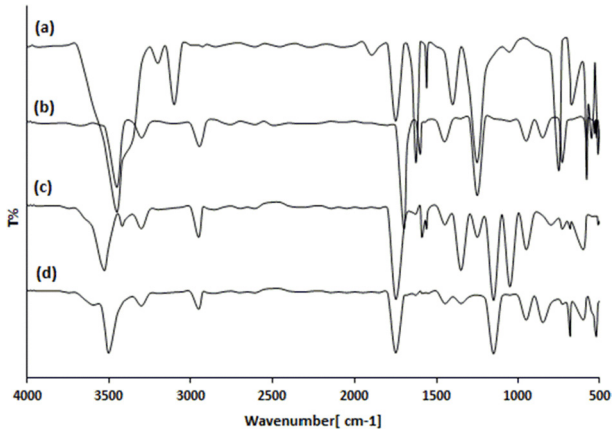

Fig. 2. FTIR spectra of synthesized (a) Gabapentin template molecule, (b) NIP-NPs, (c) leached MIP-NPs and (d) unleached MIP-NPs.

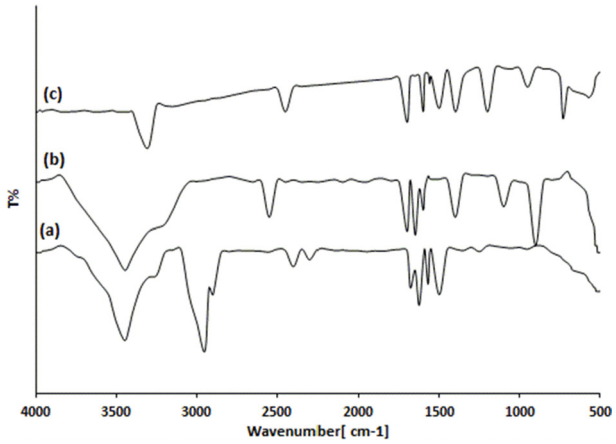

Fig. 3. FTIR spectra of (a) graphite, (b) synthesized graphene oxide and (c) GO/Ag-NPs.

3. Results and Discussion

3.1. Characterization of formed nanoparticles

3.1.1. FTIR

The FTIR spetctra of the reacting species were recorded and are presented in Figs. 2 and 3 for the GP molecule. Fig. 2a reveals the characteristic intense peaks of amine N-H stretching at 3450 cm^{-1}, O-H stretching vibration at 3200 cm^{-1}, cycloalkane C-H stretching at 3099 cm^{-1} and carbonyl C=O at 1750 cm^{-1}. C-N stretching was observed at 1250 cm^{-1}. The amino group bending vibrations were also observed at 1625 and 750 cm^{-1} for NH_2 scissoring and wagging vibrations, respectively. The FTIR spectra of the unleached MIP-NPs, shown in Fig. 2b, leached MIP-NPs, shown in Fig. 2c and NIP-NPs, shown in Fig. 2d were similar. The spectra showed peaks of carboxyl OH stretching at 3525 cm^{-1}, carbonyl C=O stretching at 1748 cm^{-1}, C-O stretching at 1250 cm^{-1} and C-H vibrations at 2951, 1450 and 1354 cm^{-1}. The peaks of the leached MIP-NPs were relatively sharper and stronger than those of NIP-NPs. This indicates the similarity of the backbone structure and shows that the template molecule had been sufficiently extracted from MIP-NPs. In the unleached MIP-NPs spectrum, the peaks of O-H and C=O were shifted to lower frequencies due to the incorporation of template molecules within the polymer cavities and the hydrogen interaction between the functional monomer hydroxyl and carbonyl groups with the GP amino and hydroxyl groups. In addition, the absence of characteristic peaks of NH2 bending vibrations at 1625 and 750 cm^{-1} in the NIP and the leached MIP-NPs spectra indicates the efficient removal of GP molecules from the MIP-NPs cavities. However, the presence of such peaks in the unleached MIP-NPs spectrum confirms the successful inclusion of the template GP molecules inside the MIP-NPs cavities.

The difference between FT-IR spectra of graphite, shown in Fig. 3a and GO, shown in Fig. 3b is the presence of a band at 1100 cm^{-1} of the C-O bond, confirming the presence of oxide functional groups after the oxidation process. In Fig. 3b, GO represented peaks of C=O and C-O vibrations at 1712 and 1011 cm^{-1}. The band at 1650 cm^{-1} indicated the presence of C=C aromatic. The peak near 1400 cm^{-1} revealed O=C-O stretching vibration. The peaks at 2550 and near 900 cm^{-1} expressed the stretching vibrations of Si-H and Si-O bonds, and indicate the successful incorporation of MPTS onto GO. The absorbed water in GO is shown by a broad peak in a range from 2953 to 3480 cm^{-1}, attributed to O-H stretching of H_2O molecules. This supports the idea that GO is a highly absorptive material, as verified by its ability to become a gel-like solution. After decoration with Ag^+ ions, as shown in Fig. 3c, it was found that the intensity of the O-H stretching vibration peak decreased due to interaction between Ag^+ ions and the oxygen-containing groups on the GO.

3.1.2. TEM and particle size distribution

Particle size distribution of the prepared NPs was studied and measured by Zeta-sizer, as shown in Fig. 4. The average diameter of Ag-NPs, shown in Fig. 4a, was 50 nm (range, 35–105 nm) while that of GO, shown in Fig. 4b, was found to be 100 nm (range, 40–120 nm). The size of GO decorated with Ag-NPs, shown in Fig. 4c, increased to 150 nm. In Fig. 4d the particle size of the prepared MIP-NPs can be seen to range from 30 to 100 nm, with an average of 50 nm. The transmission electron microscopy (TEM) images in Fig. 5a and b show the prepared Ag-NPs and the plain GO sheet, respectively. The distributions of Ag-NPs over the GO sheet and the MIP-NPs are presented in Fig. 5c and d, respectively. TEM images of the prepared NPs show their uniform spherical shapes with relatively narrow particle size distribution. The average particle diameters of GO/Ag-NPs and MIP-NPs of 80 and 65 nm, respectively, were optimum and permitted sensitive, rapid and accurate electrochemical responses

3.1.3. X-ray diffraction of synthetic materials

The X-ray diffraction (XRD) patterns of the synthesized materials are given in Fig. 6. The characteristic diffraction peak of pure crystalline graphite is found at around 26°. The XRD plot of graphene oxide synthesized by modified Hummers method showed a strong peak at 10.1° and the disappearance of the peak at 26°, which is mainly due to

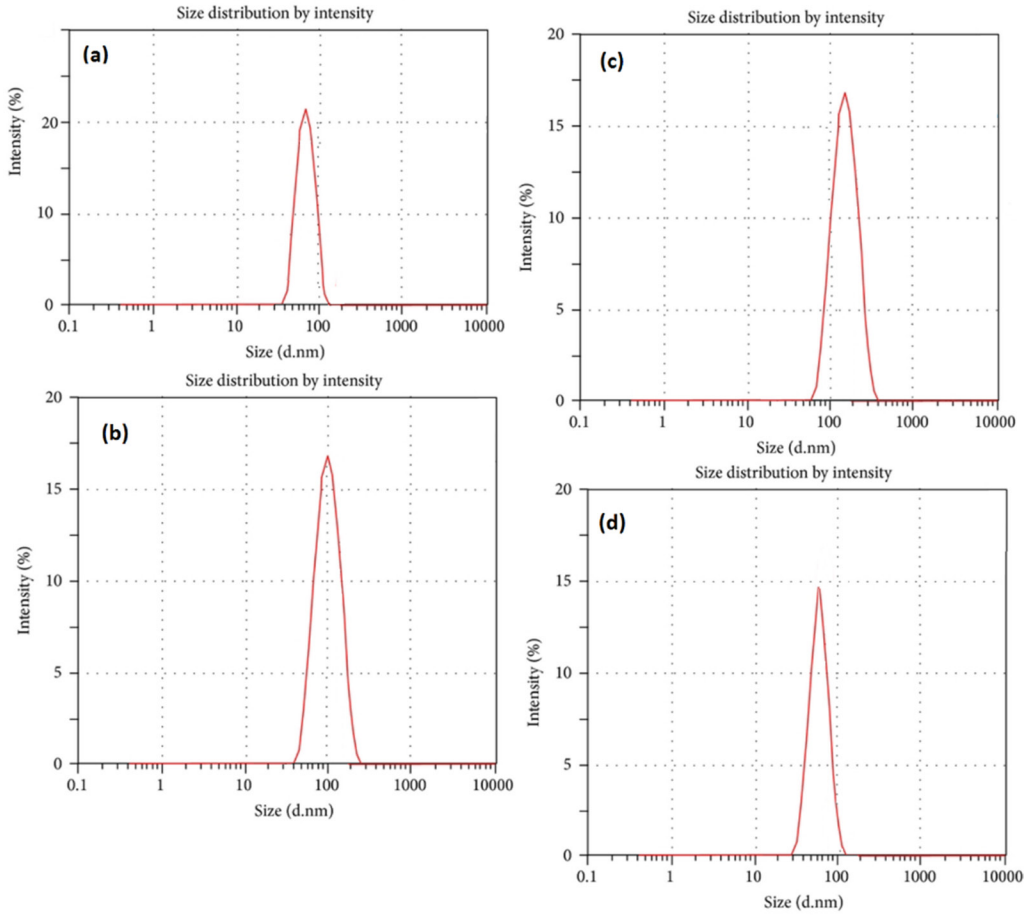

Fig. 4. Particle size distribution of (a) Ag-NPs, (b) GO-NPs, (c) GO/Ag-NPs and (d) MIP-NPs.

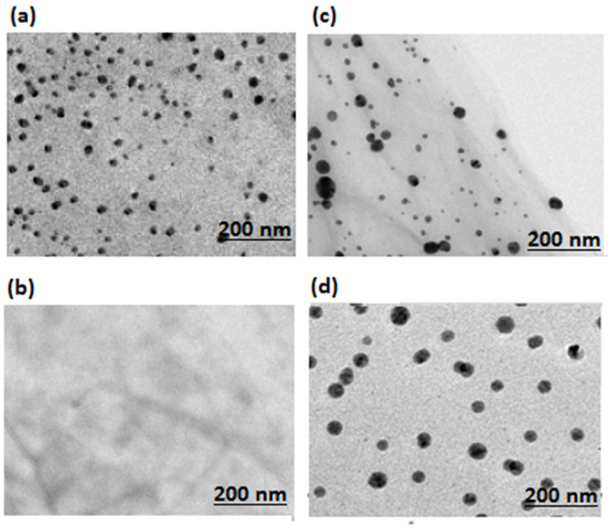

Fig. 5. TEM images of (a) Ag-NPs, (b) GO-NPs, (c) GO/Ag-NPs and (d) MIP-NPs.

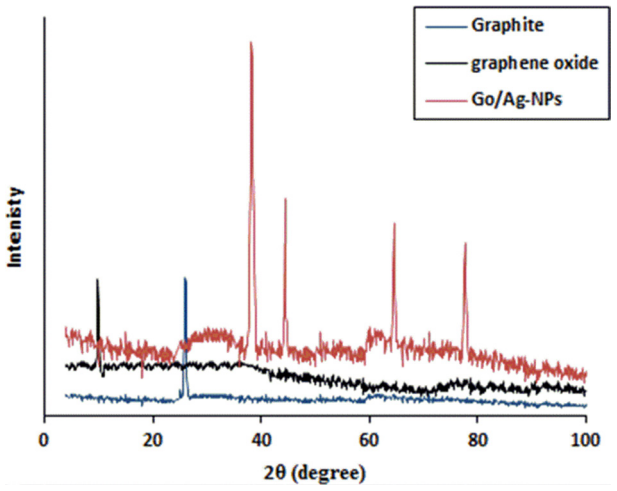

Fig. 6. Binding isotherm and Scatchard plot of synthesized MIP-NPs.

the oxidation of graphite. The results showed good agreement with the literature [41]. In the case of Ag-NP-modified GO, the characteristic diffraction peak of GO disappeared and prominent peaks at 38.2, 44.5, 64.5 and 77.6° were assigned to the crystallographic planes of Ag-NPs [44,45]. The results show that the Ag-NPs had been successfully incorporated with GO.

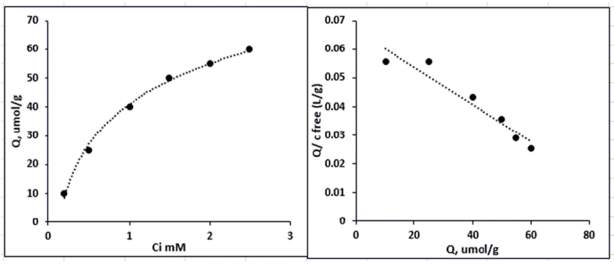

Fig. 7. XRD-pattern of graphite, GO-NPs and GO/Ag-NPs.

3.1.4. Binding study and entrapment efficiency

The interaction between GP molecules and the binding sites of MIP-NPs was studied by measuring the adsorption isotherm. This was done by plotting the binding capacity (Q) versus the free ligand concentration in the liquid phase. Q was calculated using the following equation:

$$Q = \frac{(C_i - C_f)Vs}{M} \times 1000 \quad (2)$$

, where Q is the binding capacity of MIP (μmol g^{-1}). C_i is the initial GP concentration (μmol mL^{-1}). C_f is the final GP concentration (μmol mL^{-1}). V_s is the volume of the solution (mL). M is the mass of the dried polymer. As shown in Fig. 7, the binding capacity of the MIP-NPs increased with increasing initial ligand concentration and reached saturation at higher concentrations, displaying the higher affinity for the ligand. The binding parameters were calculated by Scatchard analysis using the following equation:

$$\frac{Q}{Cfree} = \frac{[Q_{max} - Q]}{K_d} \quad (3)$$

where Q is the binding capacity. C_{free} is the free GP concentration at equilibrium. Qmax is the maximum apparent binding capacity. K_d is the dissociation constant at the binding sites. The equilibrium dissociation constant was calculated from the slope and the apparent maximum number of binding sites was calculated from the y-intercept in the linear plot of Q/C_{free} versus Q. It was found that the Scatchard plot of MIP-NPs was linear, which indicated that the binding sites are uniform and of the same affinity to GP molecules. The apparent value of K_d was found to be 1666.67 μmol L^{-1}, accompanied with site population of 111.33 μmol g^{-1} for the dry polymer.

3.2. Factors affecting formation of studied CPE

3.2.1. Effect of molar ratio of template and functional monomer

The molar ratio of the template GP and of the functional monomer influence the affinity and the imprinting efficiency of MIPs. The electrode response characteristics were measured by using different ratios. Table 1 presents the response characteristics of seven different CPEs with varying molar ratio of GP to MAA to reach the most sensitive and linear one. The results showed that MIP-NPs with a molar ratio of 1: 10 had the best recognition ability for GP and yielded the appropriate electrode response characteristics. Higher ratios led to lower sensitivity, linearity range and slope values. This may be due to agglomeration between MIP-NPs and unapproachable cavities, which led to difficult accessibility of GP molecules to the recognition sites. This idea was confirmed by measuring the particle size distribution of MIP-NPs with different molar ratios, as presented in Fig. 8. The results confirm that the smaller ratios of GP to MAA of up to 1:10, as shown in Fig. 8a-c, led to the formation of MIP-NPs with homogenous particle size distribution within 20 to 110 nm. Increasing the ratio to 1:15, as shown in Fig. 8d, and to 1:30, as shown in Fig. 8e, led to non-uniform distribution of MIP-NPs with increasing particle size that reached 1 μm, which resulted from the agglomeration of the MIP composite.

3.2.2. Effect of solvent used in synthesis of MIP-NPs

The effect of the type of the solvent used in the fabrication of the MIP-NPs was studied by measuring solvent adsorption ability. The utilized solvent affects the polymerization process. Its dissolution in the polymerization mixture provides porous structures in the MIP-NPs that enhance the binding affinity to the template molecule. Different solvents were tried in the fabrication process and the adsorption capacity (Q) of MIP-NPs for GP was determined using the previously mentioned Eq. 2.

The results in Table 2 show that MIP-NPs fabricated with acetonitrile, a porogen solvent, possessed higher adsorption binding capacity to GP molecules.

Table 1. Effect of variation of molar ratio of template to functional monomer on performance of CPE

	GP (mmol)	MAA (mmol)	EGDMA (mmol)	AIBN (mmol)	Linearity range (mol L^{-1})	LOD (mol L^{-1})	Slope (mV/decade)	Response time (s)
CPE 1	0.1	6	30	0.1	1×10^{-4} to 2×10^{-2}	1.2×10^{-5}	48.76	12
CPE 2	0.2	6	30	0.1	1×10^{-5} to 5×10^{-3}	2.5×10^{-6}	47.33	7
CPE 3	0.4	6	30	0.1	1×10^{-7} to 3×10^{-2}	3.7×10^{-8}	52.87	10
CPE 4	**0.6**	**6**	**30**	**0.1**	**1×10^{-10} to 1×10^{-3}**	**4.5×10^{-11}**	**59.86**	**15**
CPE 5	1	6	30	0.1	2×10^{-8} to 4×10^{-2}	1.7×10^{-9}	50.66	25
CPE 6	2	6	30	0.1	6×10^{-7} to 3×10^{-3}	3.5×10^{-8}	49.76	32
CPE 7	6	6	30	0.1	8×10^{-5} to 7×10^{-2}	2.8×10^{-6}	43.56	35

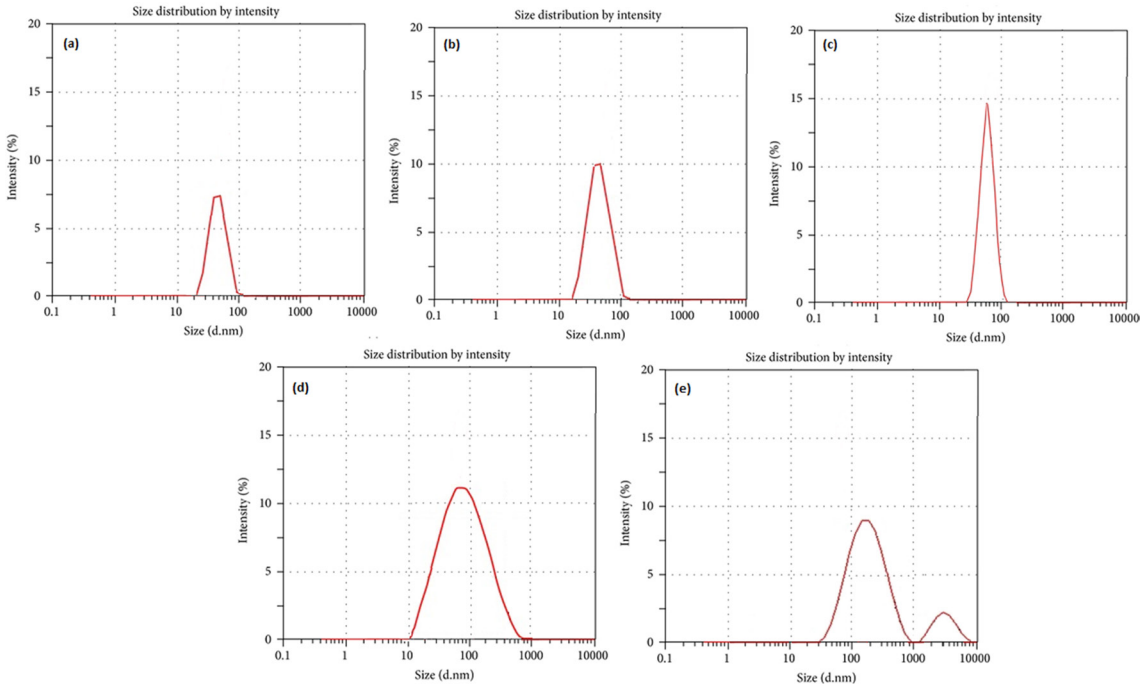

Fig. 8. Particle size distribution of MIP-NPs with different molar ratios of GP to MAA of (a) 1:3, (b) 1:6, (c) 1: 10, (d) 1:15, and (e) 1: 30.

Table 2. Adsorption binding capacity of MIP-NPs using different porogen solvents

MIP-NPs	Porogen solvent	Adsorption capacity (Q)
1	DMSO	53.38
2	Chloroform	58.36
3	Ethanol	51.24
4	Acetonitrile	70.00

Table 3. Gabapentin recovery percentage after using different washing solvents

Washing solvent	Gabapentin recovery (%)
Acetonitrile	68
Deionized water	29
Methanol : acetic acid (9:1 v/v)	94.2
Britton-Robinson pH 5	73
Tetrahydrofuran	55

3.2.3. Effect of washing time and washing solvent on electrode performance

The most suitable washing solvent is the one that can elute the accumulated GP template molecule from MIP-NPs cavities without affecting the CPE matrix. Different washing solvents were tried and the most appropriate one was chosen. The recovery percentage of GP in the washing solvent was estimated by using the HPLC method to determine the amount of GP in the washing extract [18]. As shown in Table 3, the most appropriate solvent, with the highest recovery, is a mixture of methanol and acetic acid (9:1 v/v). It shows good template solubility and high ability to break the interaction between the template and the binding cavities of MIP-NPs. The suitability of the methanol: acetic acid mixture might be due to its lower pH, which does not favor template adsorption onto MIP-NPs. By increasing the time of washing the CPE, the electrochemical response decreased to 15.5% of its initial response after washing for 2 min, as presented in Fig. 9.

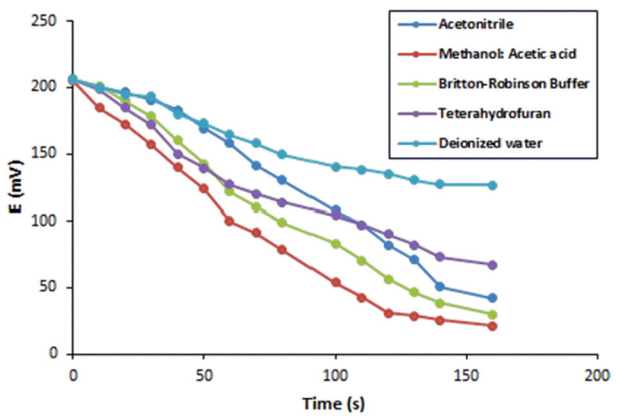

Fig. 9. Electrochemical response after washing electrode with different solvents at different time intervals using 10^{-6} M GP solution.

3.2.4. Effect of GO/Ag-NPs on performance of studied CPE

Bare CPE suffered a limited response in the determination of GP. Incorporation of MIP-NPs enhanced the recognition ability of the synthesized electrode and augmented the template molecule potential. This is due to the great recogni-

Table 4. Optimization of electrochemical composition of studied CPE

CPE	Electrode composition (% w/w)				Slope (mV/concentration decade)	Linearity range (mol L^{-1})	Response time (s)	LOD (mol L^{-1})
	Graphite	MIP-NPs	GO/Ag-NPs	Paraffin oil				
1	75	-	-	25	47.45	1×10^{-2} to 1×10^{-3}	25	6.5×10^{-4}
2	60	15	-	25	53.83	1×10^{-2} to 1×10^{-4}	32	8.2×10^{-7}
3	55	20	-	25	52.33	1×10^{-2} to 1×10^{-7}	35	9.3×10^{-5}
4	50	25	-	25	53.26	1×10^{-2} to 1×10^{-7}	35	4.6×10^{-6}
5	35	25	15	25	55.78	1×10^{-2} to 1×10^{-8}	25	8.6×10^{-7}
6	20	25	30	25	56.29	1×10^{-2} to 1×10^{-9}	19	6.3×10^{-7}
7	**20**	**25**	**35**	**20**	**59.86**	**1×10^{-3} to 1×10^{-10}**	**15**	**4.5×10^{-11}**
8	20	30	35	15	56.45	1×10^{-4} to 1×10^{-8}	15	4.9×10^{-9}
9	25	40	10	25	53.65	1×10^{-2} to 1×10^{-8}	23	2.6×10^{-9}
10	20	20	30	30	54.78	1×10^{-2} to 1×10^{-7}	20	3.7×10^{-8}
11	20	25	40	15	57.45	1×10^{-2} to 1×10^{-9}	13	6.2×10^{-10}
12	30	20	30	20	57.66	1×10^{-3} to 1×10^{-8}	10	2.8×10^{-9}
13	20	15	35	30	58.45	1×10^{-2} to 1×10^{-9}	10	8.1×10^{-10}

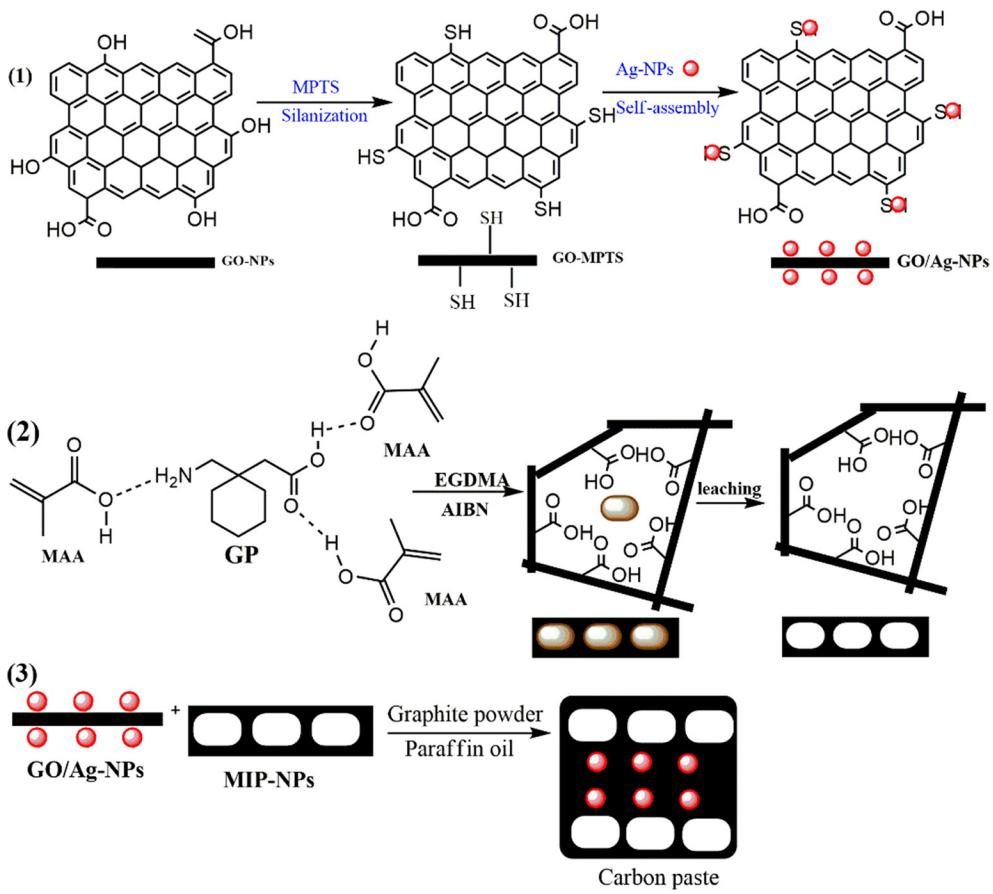

Fig. 10. Illustration of fabrication procedure for GO/Ag-NPs and MIP-NPs.

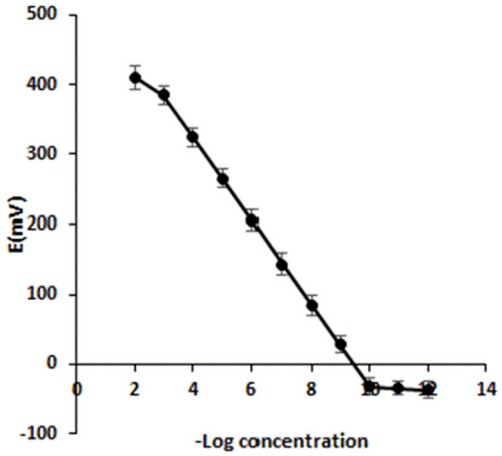

Fig. 11. Potentiometric calibration profile of gabapentin sensor.

tion ability of MIP-NPs to accumulate GP molecules on the electrode surface. As can be seen in Table 4, increasing the percentage of MIP-NPs largely did not enhance the electrode behavior, as expected. The response time increased with increasing MIP-NP concentration. This may be explained by the insulating effect of MIP-NPs [46]. Although the MIP-NPs have high recognition power, their insulating nature affects the CPE response characteristics. Go/Ag-NPs were applied in combination with MIP-NPs to improve the electrode performance. The combined materials enhance the electron transfer rate of the electrochemical reaction and the stability of the sensor. GO has had a great impact in electrochemical field due to its high dispersibility, ease of production and coupling capability. The use of GO is limited only by its poor electrical conductivity [47]. Metal and metal oxide NPs are characterized by their catalytic and electronic properties and good biocompatibility. They are widely used in electrochemical sensor fabrication [48,49]. The combination of GO and Ag-NPs provided fast mass transport to the binding sites and high surface area. This led to decreases in the diffusion barrier and the binding time. Different CPEs with different composition percentages were fabricated and their response characteristics were recorded. As shown in Table 4, the most appropriate CPE is the one that is prepared by a mixture of graphite powder, MIP-NPs, GO/Ag-NPs and paraffin oil in a ratio (4%:5%:7%:4% w/w). An illustration of the fabrication procedure of the CPE is presented in Fig. 10. This proposed CPE revealed the best performance, with a linearity range from 1×10^{-3} to 1×10^{-10} mol L^{-1} and a slope value of 59.86 (mV/concentration decade), as shown in Fig. 11; this is the ideal slope of a monovalent cation.

3.3. Sensor performance

3.3.1. Electrode conditioning and regeneration

The freshly-prepared sensor surface was conditioned in 1×10^{-5} mol L^{-1} GP pH 2 solution for 36 h. Then, the electrode was washed with a mixture of methanol and acetic acid (9:1 v/v%), followed by deionized water for 2 min; electrode was then used successfully for more than 15 determinations of different concentrations without any deterioration of the electrode potential. Returning the response of the electrode to its initial potential requires repeated washing with the washing solvent.

3.3.2. Dynamic response time and lifetime of studied CPE

After increasing GP concentration 10-fold, the time required for the electrode to reach a stable potential reading was controlled by use of the proper washing solvent, as mentioned previously. While measuring the concentrations of GP from low to high and from high to low, as graphically represented in Fig. 12, the electrode potential remained

Table 5. Effect of soaking time and lifetime of studied CPE

Electrode composition	Time	Slope (mV/decade)	Concentration range (mol L^{-1})	Response time (s)
CPE 1 20 mg graphite powder+35 mg GO/Ag-NPs + 25 mg MIP-NPs + 0.02 g paraffin oil	1 h	46.45	1.0×10^{-7} to 1.0×10^{-3}	35
	6 h	48.61	1.0×10^{-7} to 1.0×10^{-3}	27
	24 h	53.38	1.0×10^{-9} to 1.0×10^{-3}	13
	36 h	**59.32**	**1.0×10^{-10} to 1.0×10^{-3}**	**15**
	48 h	59.16	1.0×10^{-10} to 1.0×10^{-3}	18
	8 d	58.74	1.0×10^{-10} to 1.0×10^{-3}	16
	26 d	59.33	1.0×10^{-10} to 1.0×10^{-3}	15
	39 d	58.42	1.0×10^{-10} to 1.0×10^{-3}	15
	64 d	58.16	1.0×10^{-10} to 1.0×10^{-3}	15
	88 d	59.76	1.0×10^{-10} to 1.0×10^{-3}	18
	115 d	**59.87**	**1.0×10^{-10} to 1.0×10^{-3}**	**16**
	128 d	51.43	1.0×10^{-8} to 1.0×10^{-3}	12
	142 d	46.5	1.0×10^{-6} to 1.0×10^{-3}	21

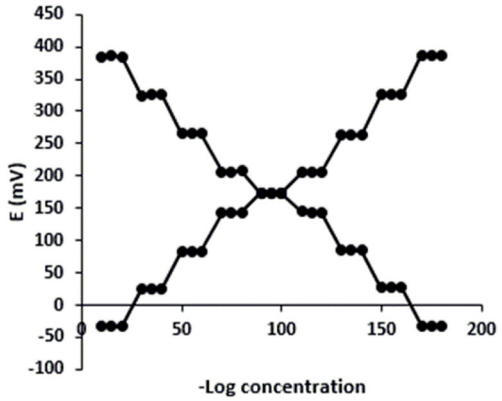

Fig. 12. Dynamic response time of gabapentin sensor from low to high and high to low concentrations.

unaffected. It is evident that the response of the studied sensor was rapid and reversible. The studied sensor exhibited a fast dynamic response ≤17 s from low to high concentrations, although the time required to reach equilibrium from the high to the low sample concentration was longer than ≤90 s. The calibration slope, response time and linearity range of the proposed sensor were recorded over a period of 142 d, without any surface renewal. Resulting values were reproducible within ±5% of the original values for a period of 115 d, as demonstrated in Table 5. The electrochemical response characteristics of the studied sensor are summarized in Table 6. A comparison between the studied electrode and other reported electrochemical sensors is presented in Table 7. It reveals the superiority of the proposed sensor in the determination of GP with high sensitivity, stability and accuracy.

Table 6. Electrochemical performance characteristics of studied CPE

Parameter	Value
Slope (mV/decade)	59.86
LOD (mol L^{-1})[a)]	4.8×10^{-11}
Response time (s)	15
Working pH range	1.5–3
Concentration range (mol L^{-1})	1×10^{-10} to 1×10^{-3}
Stability (d)	115
Average recovery±SD (%)[b)]	98.41±0.78
Correlation coefficient	0.9992
Repeatability (RSD)	0.83
Intermediate precision (RSD)	0.94
Ruggedness[c)]	97.24±1.21

[a)]Limit of detection (measured by intersection of extrapolated arms of potential profile figure).
[b)]Average of five determinations.
[c)]Average recovery percent to determine (10^{-7}, 10^{-5} and 10^{-3} M) for the proposed sensor using Mettler Toledo MP225digital ion analyzer instead of clean PH 600 digital ion analyzer.

3.3.3. Effect of pH

The influence of pH on the response of the proposed sensor was studied over a pH range of 0.5–5.0, adjusted with either HCl or NaOH. As shown in Fig. 13, at low pH values, the potential was increased and the electrode responded to H^+ ions and GP cations simultaneously. The electrode response

Table 7. Comparison of electrochemical methods of GP determination

Method	Electrode	Linear range (mol L^{-1})	LOD (mol L^{-1})	Reference
CV, DPV	Gold electrode	0.3×10^{-6} to 15×10^{-6}	0.13×10^{-6}	[26]
CV	CPE modified with nickel oxide nanotubes	2.4×10^{-6} to 5×10^{-5}	0.3×10^{-6}	[25]
CV	Carbon ceramic electrode (CCE) modified with nickel-catechol complex (Ni-CA)	1.25×10^{-6} to 6.32×10^{-5}	0.5×10^{-6}	[23]
CV, DPV	Carbon paste electrode modified with copper sulfide nanostructures	5×10^{-6} to 5.5×10^{-5}	0.5×10^{-6}	[22]
CV	Carbon nanotube bed electrode impregnated with silver–nanoparticles (Ag-NPs)	3.1×10^{-9} to 2.9×10^{-2}	5.6×10^{-10}	[24]
Potentiometry	PVC membrane with gabapentin phosphomolybdic acid ion pair complex	1×10^{-5} to 5×10^{-2}	1×10^{-5}	[27]
Potentiometry	Plastic membrane (I) , coated wire (II) and coated graphite rod (III) with incorporation of gabapentin with phosphotungstic acid	1×10^{-5} to 1×10^{-2} (I) 5×10^{-6} to 1×10^{-2} (II) 1×10^{-5} to 9×10^{-3} (III)	5×10^{-6} (I) 2.5×10^{-6} (II) 4.6×10^{-6} (III)	[28]
Potentiometry	CPE with graphene oxide/silver nanoparticles with molecular imprinted nanoparticles	1×10^{-10} to 1×10^{-3}	4.8×10^{-11}	This work

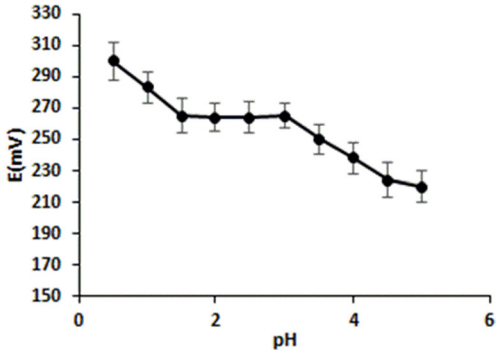

Fig. 13. Effect of pH on response of studied gabapentin sensor.

Table 8. Selectivity coefficients of GP sensor with interfering ions

Interfering ions	-log $K^{pot}_{GP,\ interferent}$
Urea	4.56
Na^{+}	5.27
Li^{+}	4.29
Ca^{2+}	5.44
Mg^{2+}	5.31
Cu^{2+}	5.09
Glucose	4.86
Lactose	4.29
L-cysteine	3.67
L-Lucien	3.72
Phenylalanine	4.56
Caffeine	4.16
Diazepam	3.85
Baclofen	4.62
Pseudoephedrine	4.39
Pregabalin	4.68

was maintained constant over a pH range of 1.5–3.0. At higher pH, the potential decreased because of the formation of carboxylate anion of GP; also, the carboxylate was situated on the polymer that ionized at pH values higher than pKa of MAA (4.7) and did not interact with the template molecule. pH 2 was chosen as a suitable pH for measurements using 0.01 M citrate buffer.

3.3.4. Selectivity coefficient of studied CPE

The selectivity towards GP of the proposed sensor was studied with respect to structurally related molecules such as Pregabalin, baclofen and amino acids, and other interfering ions. This was done by using the separate solution method to calculate the selectivity coefficient. The obtained data are summarized in Table 8. The results confirm that the electrode was highly selective for the determination of GP in the presence of either interfering ions or structurally related molecules.

Table 9. Determination of GP by applying standard addition method

	GO/Ag/MIP-NPs sensor		
	Gabapentin (mol L^{-1})	Recovery (%)	RSD
Pure solution	6×10^{-3}	98.34	1.02
	3×10^{-4}	99.02	0.95
	5×10^{-6}	100.13	0.83
	2×10^{-8}	98.37	1.15
	1×10^{-7}	99.67	0.91
Average±SD		99.11±0.79	
N		5	
Variance		0.62	
F-test (5.19)[a)]		1.45	
Student t test (2.262)[a)]		0.48	
Neurontin Tablet	4×10^{-5}	97.78	0.85
	3×10^{-6}	99.27	0.76
	6×10^{-4}	98.39	0.92
	6×10^{-8}	99.06	1.06
	3×10^{-7}	98.72	1.21
Average±SD		98.64±0.59	
N		5	
Variance		0.35	
F-test (5.19)[a)]		1.66	
Student t test (2.262)[a)]		1.65	

[a)]The values in parentheses are the corresponding theoretical values of t and F at the 95% confidence level.
N.B.: The reported method [18]; Average±SD (99.36±0.95), n=6 for pure solution and (99.31±0.76), n=6 for pharmaceutical dosage form.

3.4. Analytical applications

The studied GP sensor was successfully applied for the determination of GP in bulk and pharmaceutical formulation with acceptable recovery and accuracy. Comparison of the studied sensor with one for the reported method [18] revealed no significant difference, as shown in Table 9.

In addition, the GP sensor was effectively applied for the determination of spiked human plasma; sensor showed high accuracy and sensitivity, as indicated in Table 10, which enables this sensor to be used in GP bioequivalence and clinical studies.

Table 10. Accuracy and precision of GP in spiked human plasma

Plasma concentration ($\mu g\ mL^{-1}$)	Calculated mean plasma concentration ($\mu g\ mL^{-1}$)	SD	CV (%)	Recovery (%)	RE (%)
Intra-day					
0.1	0.100	0.003	2.71	99.60	0.40
0.5	0.496	0.018	3.66	99.20	0.80
1	0.998	0.016	1.65	99.80	0.20
2.5	2.490	0.024	0.98	99.60	0.40
4	3.950	0.044	1.10	98.75	1.25
6	5.948	0.056	0.95	99.13	0.87
Inter-day					
0.1	0.098	0.001	1.32	98.00	2.00
0.5	0.490	0.017	3.49	98.00	2.00
1	0.990	0.022	2.24	99.00	1.00
2.5	2.487	0.041	1.64	99.47	0.53
4	4.030	0.043	1.08	100.75	–0.75
6	5.910	0.056	0.94	98.50	1.50

[a)]Average of five determinations.
SD, standard deviation; CV, coefficient of variation; RE, relative error.

4. Conclusions

GP, an antiepileptic drug, is successfully determined using CPE modified with GO/Ag-NPs and MIP-NPs. The incorporation of Go/Ag-NPs enhances the electrochemical characteristics of the molecularly imprinted sensor; it enhances the electron transfer, minimizes the insulating effect of MIP-NPs and improves the selectivity towards the template molecule. The proposed sensor is successfully applied for the determination of GP in bulk, pharmaceutical formulations and plasma samples. It shows high sensitivity and stability, and wide linearity range.

Conflict of Interest

No potential conflict of interest relevant to this article was reported.

References

[1] Stein D, Lydiard RB, Giordano S, Mandel F. Poster session II : benzodiazepine and anxiolytics. Eur Psychiatry, **23**, S221 (2008). https://doi.org/10.1016/j.eurpsy.2008.01.389.

[2] Petroff OAC, Hyder F, Rothman DL, Mattson RH. Effects of gabapentin on brain GABA, homocarnosine, and pyrrolidinone in epilepsy patients. Epilepsia, **41**, 675 (2000). https://doi.org/10.1111/j.1528-1157.2000.tb00227.x.

[3] Tampi RR, Ozkan B, Williamson D. Gabapentin for the treatment of behavioral and psychological symptoms of dementia. Adv Alzheimer's Dis, **1**, 13 (2012). https://doi.org/10.4236/aad.2012.12002.

[4] Siddiqui FA, Arayne MS, Sultana N, Qureshi F, Mirza AZ, Zuberi MH, Bahadur SS, Afridi NS, Shamshad H, Rehman N. Spectrophotometric determination of gabapentin in pharmaceutical formulations using ninhydrin and π-acceptors. Eur J Med Chem, **45**, 2761 (2010). https://doi.org/10.1016/j.ejmech.2010.02.058.

[5] Ambalal PS, Natavarlal JP. Visible spectrophotometric methods for determination of gabapentin in pharmaceutical tablet and capsule dosage forms. Asian J Pharm Life Sci, **1**, 223 (2011).

[6] Mohammed TO, Elbashir AA. Spectrophotometric method for determination of gabapentin in pharmaceutical formulation by derivatization with 4-chloro-7-nitrobenzo-2-oxa-1,3-diazole (NBD-Cl). Int J Drug Dev Res, **7**, 1 (2015).

[7] Effendi N, Rachmat K, Akbar P, Tadjuddin N. Validated UV-Vis spectrophotometric method for determination of gabapentin using acetyl acetone and formaldehyde reagents. Iran J Pharm Sci, **9**, 23 (2013).

[8] Saleh MS, Youssef AK, Hashem EY, Abdel-kader DA. A novel spectrophotometric method for determination of gabapentin in pharmaceutical formulations using 2,5-dihydroxybenzaldehyde. Comput Chem, **2**, 22 (2014). https://doi.org/10.4236/cc.2014.22004.

[9] Abdulrahman SAM, Basavaiah K. Highly sensitive spectrophotometric method for the determination of gabapentin capsules using sodium hypochloride. Turk J Pharm Sci, **9**, 113 (2012).

[10] Abdellatef HE, Khalil HM. Colorimetric determination of gabapentin in pharmaceutical formulation. J Pharm Biomed Anal, **31**, 209 (2003). https://doi.org/10.1016/s0731-7085(02)00572-1.

[11] Al-Majed AA. A derivatization reagent for vigabatrin and gabapentin in HPLC with fluorescence detection. J Liq Chromatogr Relat Technol, **28**, 3119 (2005). https://doi/org/10.1080/10826070500295229.

[12] Patel Y, Patel MB, Patel NK, Sakhreliya B. Development and validation of analytical method for simultaneous estimation of gabapentin and nortriptyline hydrochloride in pharmaceutical dosage form. J Pharm Sci Bioscientific Res, **5**, 434 (2015).

[13] Jalalizadeh H, Souri E, Tehrani MB, Jahangiri A. Validated HPLC method for the determination of gabapentin in human plasma using pre-column derivatization with 1-fluoro-2,4-dinitrobenzene and its application to a pharmacokinetic study. J Chromatogr B, **854**, 43 (2007). https://doi/org/10.1016/j.jchromb.2007.03.039.

[14] Hyder S, Vani R. Stability indicating method development and validation of RP-HPLC method for simultaneous estimation of gabapentin and mecobalamine in bulk and its tablets. World J Pharm Pharm Sci, **3**, 1095 (2014).

[15] Ragham PK, Chandrasekhar KB. Development and validation of a stability-indicating RP-HPL C-CAD method for gabapentin and its related impurities in presence of degradation products. J Pharm Biomed Anal, **125**, 122 (2016). https://doi.org/10.1016/j.jpba.2016.03.035.

[16] Ciavarella AB, Gupta A, Sayeed VA, Khan MA, Faustino PJ. Development and application of a validated HPLC method for the determination of gabapentin and its major degradation impurity in drug products. J Pharm Biomed Anal, **43**, 1647 (2007). https://doi.org/10.1016/j.jpba.2006.12.020.

[17] Sagirli O, Cetin SM, Önal A. Determination of gabapentin in human plasma and urine by high-performance liquid chromatography with UV–vis detection. J Pharm Biomed Anal, **42**, 618 (2006). https://doi/org/10.1016/j.jpba.2006.05.012.

[18] Gupta A, Ciavarella AB, Sayeed VA, Khan MA, Faustino PJ. Development and application of a validated HPLC method for the analysis of dissolution samples of gabapentin drug products. J Pharm Biomed Anal, **46**, 181 (2008). https://doi.org/10.1016/j.jpba.2007.08.023.

[19] Park JH, Jhee OH, Park SH, Lee JS, Lee MH, Shaw LM, Kim KH, Lee JH, Kim YS, Kang JS. Validated LC-MS/MS method for quantification of gabapentin in human plasma: application to pharmacokinetic and bioequivalence studies in Korean volunteers. Biomed Chromatogr, **21**, 829 (2007). https://doi.org/10.1002/bmc.826.

[20] Carlsson KC, Reubsaet JLE. Sample preparation and determination of gabapentin in venous and capillary blood using liquid chromatography–tandem mass spectrometry. J Pharm Biomed Anal, **34**, 415 (2004). https://doi.org/10.1016/s0731-7085(03)00572-7.

[21] Borrey DCR, Godderis KO, Engelrelst VIL, Bernard DR, Langlois MR. Quantitative determination of vigabatrin and gabapentin in human serum by gas chromatography–mass spectrometry. Clin Chim Acta, **354**, 147 (2005). https://doi.org/10.1016/j.cccn.2004.11.023.

[22] Nezhad GK, Pashazadeh S. Electro-oxidation and determination of gabapentin at copper sulfide nanostructures modified carbon paste electrode. Anal Bioanal Electrochem, **7**, 439 (2015).

[23] Jalali F, Hassanvand R, Dorraji PS. Voltammetric Determination of gabapentin by a carbon ceramic electrode modified with multiwalled carbon nanotubes and nickel-catechol complex. J Braz Chem Soc, **25**, 1537 (2014). https://doi.org/10.5935/0103-5053.20140137.

[24] Yari A, Papi F, Farhadi S. Voltammetric determination of trace antiepileptic gabapentin with a silver-nanoparticle modified multiwalled carbon nanotube paste electrode. Electroanalysis, **23**, 2949 (2011). https://doi.org/10.1002/elan.201100454.

[25] Heli H, Faramarzi F, Sattarahmady N. Oxidation and determination of Gabapentin on nanotubes of nickel oxide-modified carbon paste electrode. J Solid State Electrochem, **16**, 45 (2010). https://doi.org/10.1007/s10008-010-1272-9.

[26] Hegde RN, Swamy BEK, Shetti NP, Nandibewoor ST. Electrooxidation and determination of gabapentin at gold electrode. J Electroanal Chem, **635**, 51 (2009). https://doi.org/10.1016/j.jelechem.2009.08.004.

[27] Jalali F, Arkan E, Bahrami G. Preparation of a gabapentin potentiometric sensor and its application to pharmaceutical analysis. Sens Actuators B Chem, **127**, 304 (2007). https://doi.org/10.1016/j.snb.2007.07.019.

[28] El-Tohamy M, Razeq S, Shalaby A. Electrochemical sensors for determination of anticonvulsant drug gabapentin in bulk powder and pharmaceutical dosage forms. Int J Electrochem Sci, **7**, 5374 (2012).

[29] Zhu Y, Yang L, Huang D, Zhu Q. Molecularly imprinted nanoparticles and their releasing properties, bio-distribution as drug carriers. Asian J Pharm Sci, **12**, 172 (2017). https://doi.org/10.1016/j.ajps.2016.08.008.

[30] Tan F, Zhao Q, Teng F, Sun D, Gao J, Quan X, Chen J. Molecularly imprinted polymer/mesoporous carbon nanoparticles as electrode sensing material for selective detection of ofloxacin. Mater Lett, **129**, 95 (2014). https://doi.org/10.1016/j.matlet.2014.05.039.

[31] Arabi M, Ghaedi M, Ostovan A, Tashkhourian J, Asadallahzadeh H. Synthesis and application of molecularly imprinted nanoparticles combined ultrasonic assisted for highly selective solid phase extraction trace amount of celecoxib from human plasma samples using design expert (DXB) software. Ultrason Sonochem, **33**, 67 (2016). https://doi.org/10.1016/j.ultsonch.2016.04.022.

[32] Atar N, Yola ML, Eren T. Sensitive determination of citrinin based on molecular imprinted electrochemical sensor. Appl Surf Sci, **362**, 315 (2016). https://doi.org/10.1016/j.apsusc.2015.11.222.

[33] Yola ML, Eren T, Atar N. A sensitive molecular imprinted electrochemical sensor based on gold nanoparticles decorated graphene oxide: application to selective determination of tyrosine in milk. Sens Actuators B Chem, **210**, 149 (2015). https://doi.org/10.1016/j.snb.2014.12.098.

[34] Yola ML, Atar N. A highly efficient nanomaterial with molecular imprinting polymer: carbon nitride nanotubes decorated with graphene quantum dots for sensitive electrochemical determination of chlorpyrifos. J Electrochem Soc, **164**, B223 (2017). https://doi.org/10.1149/2.1411706jes.

[35] Li J, Wei G, Zhang Y. Molecularly imprinted polymers as recognition elements in sensors. Mol Imprinted Sens, 35 (2012). https://doi.org/10.1016/b978-0-444-56331-6.00002-5.

[36] Javanbakht M, Akbari-Adergani B. Molecularly Imprinted Polymer-Based Potentiometric Sensors for the Determination of Drugs in Pharmaceutical, Biological, and Environmental Samples. Mol Imprinted Sens, 247 (2012). https://doi.org/10.1016/b978-0-444-56331-6.00011-6.

[37] Alam SN, Sharma N, Kumar L. Synthesis of Graphene Oxide (GO) by Modified Hummers Method and Its Thermal Reduction to Obtain Reduced Graphene Oxide (rGO). Graphene, **6**, 1 (2017). https://doi.org/10.4236/graphene.2017.61001.

[38] Ma J, Zhang J, Xiong Z, Yong Y, Zhao XS. Preparation, characterization and antibacterial properties of silver-modified graphene

oxide. J Mater Chem, **21**, 3350 (2011). https://doi.org/10.1039/c0jm02806a.

[39] Zhang Y, Liu S, Wang L, Qin X, Tian J, Lu W, Chang G, Sun X. One-pot green synthesis of Ag nanoparticles-graphene nanocomposites and their applications in SERS, H_2O_2, and glucose sensing. RSC Adv, **2**, 538 (2012). https://doi.org/10.1039/c1ra00641j.

[40] Chen C, Fu X, Ma T, Fan W, Wang Z, Miao S. Synthesis and electrochemical properties of graphene oxide/nanosulfur/polypyrrole ternary nanocomposite hydrogel for supercapacitors. J Appl Polym Sci, **131**, 40814 (2014). https://doi.org/10.1002/app.40814.

[41] Shahriary L, Athawale AA. Graphene oxide synthesized by using modified hummers approach. Int J Renew Energy Environ Eng, **2**, 58 (2014).

[42] Umezawa Y, Bühlmann P, Umezawa K, Tohda K, Amemiya S. Potentiometric selectivity coefficients of ion-selective electrodes. Part I. inorganic cations (technical report). Pure Appl Chem, **72**, 1851 (2000). https://doi.org/10.1351/pac200072101851.

[43] Baumann EW. Trace fluoride determination with specific ion electrode. Anal Chim Acta, **42**, 127 (1968). https://doi.org/10.1016/s0003-2670(01)80277-4.

[44] Jyoti K, Baunthiyal M, Singh A. Characterization of silver nanoparticles synthesized using Urtica dioica Linn. leaves and their synergistic effects with antibiotics. J Radiat Res Appl Sci, **9**, 217 (2016). https://doi.org/10.1016/j.jrras.2015.10.002.

[45] Hui KS, Hui KN, Dinh DA, Tsang CH, Cho YR, Zhou W, Hong X, Chun HH. Green synthesis of dimension-controlled silver nanoparticle–graphene oxide with in situ ultrasonication. Acta Mater, **64**, 326 (2014). ttps://doi.org/10.1016/j.actamat.2013.10.045.

[46] Alizadeh T, Azizi S. Graphene/graphite paste electrode incorporated with molecularly imprinted polymer nanoparticles as a novel sensor for differential pulse voltammetry determination of fluoxetine. Biosens Bioelectron, **81**, 198 (2016). https://doi.org/10.1016/j.bios.2016.02.052.

[47] Chen D, Feng H, Li J. Graphene oxide: preparation, functionalization, and electrochemical applications. Chem Rev, **112**, 6027 (2012). https://doi.org/10.1021/cr300115g.

[48] Luo X, Morrin A, Killard AJ, Smyth MR. Application of nanoparticles in electrochemical sensors and biosensors. Electroanalysis, **18**, 319 (2006). https://doi.org/10.1002/elan.200503415.

[49] Ren X, Meng X, Chen D, Tang F, Jiao J. Using silver nanoparticle to enhance current response of biosensor. Biosens Bioelectron, **21**, 433 (2005). https://doi.org/10.1016/j.bios.2004.08.052.